AIAA-2003-0728

EFFECT OF AIRFOIL GEOMETRY ON PERFORMANCE WITH SIMULATED INTERCYCLE ICE ACCRETIONS

Andy P. Broeren* and Michael B. Bragg†

University of Illinois at Urbana-Champaign, Urbana, IL 61801

Abstract

This paper presents the results of an experimental study designed to evaluate the performance effects of intercycle ice accretions on airfoils with different geometries. The intercycle ice accretions were simulated using combinations of various size grit roughness. These simulations were tested on three airfoils: NACA 23012, NACA 3415 and NLF 0414 at a Reynolds number of 1.8×10^6 and a Mach number of 0.18. Results from the NACA 23012 airfoil tests closely matched those from a previous study, validating the ice-shape simulation method. This also showed that a simple geometric (chord-based) scaling of the ice was appropriate. The simulated ice effect, in terms of maximum lift performance, was most severe for the NACA 23012 airfoil. The maximum lift coefficients were in the range of 0.65 to 0.80 for the iced configuration compared to a clean value of 1.47 for the NACA 23012 airfoil at this Reynolds number. In contrast, the maximum lift coefficients for the NLF 0414 airfoil with the same ice simulations were in the range of 0.90 to 1.05, compared to a clean value of 1.34. The results for the NACA 3415 with the simulated intercycle ice shapes were between the other two airfoils.

Nomenclature

α	Airfoil angle of attack
α_{stall}	Stalling angle of attack, coincident with $C_{l,max}$
c	Airfoil chord length
C_d	Drag coefficient
C_l	Lift coefficient
$C_{l,max}$	Maximum lift coefficient, coincident with α_{stall}
C_m	Quarter-chord pitching-moment coefficient
C_p	Pressure coefficient
k	Roughness height or thickness
Ma	Freestream Mach number
Re	Freestream Reynolds number, based on chord
t	Airfoil maximum thickness
x	Chordwise position along airfoil
y	Normal position from airfoil chord line

Introduction

The cyclic operation of typical pneumatic aircraft deicing systems leads to the formation of residual and intercycle ice accretions. For example, pneumatic boots are usually inflated and deflated at either one-minute or three-minute intervals, depending upon the severity of icing. The ice accretion present on the deicer surface just prior to its initial activation is the "preactivation" ice. After the system has been cycled a sufficient number of times, the periodic activation and ice accretion cycle reaches steady state. After steady state has been reached, "intercycle" ice refers to the ice shape as it exists immediately *before* subsequent activations of the deicer. This is not to be confused with "residual" ice which refers to any ice that remains on the surface immediately *after* the deicer operation. This paper addresses the aerodynamic performance penalties associated with intercycle ice accretions for three different airfoil geometries.

The characteristics of residual and intercycle ice accretions have been the subject of several previous investigations. Shin and Bond[1] analyzed the ice accretions for several different deicing systems installed on a NACA 0012 airfoil model. The reported results were mainly for one minute cycling times and showed that the deicers generally cleaned the leading edge, leaving little residual ice. The height of the intercycle ice roughness, normalized by chord, varied from approximately $k/c = 0.002$ to 0.010, depending upon the icing condition (i.e., glaze or rime) and the type of deicer. Shin and Bond[1] concluded that the intercycle ice would have an effect on airfoil and wing performance and that uniformly distributed roughness

* Research Scientist, Dept. of Aeronautical and Astronautical Eng., Univ. of Illinois, Member AIAA.
† Professor and Head, Dept. of Aeronautical and Astronautical Eng., Univ. of Illinois, Associate Fellow, AIAA.

may not be an appropriate simulation of the actual intercycle ice. No aerodynamic measurements were performed during the study.

Aerodynamic performance effects of residual and intercycle ice were included in some of the previous research. Albright *et al.*[2] measured the drag coefficient before and after the operation of pneumatic deicer on a NACA 65_1-215 airfoil. The general results showed that the intercycle ice (before deicer operation) resulted in a higher drag coefficient than the residual ice (after deicer operation), both of which were higher than for the clean airfoil. Similar research was carried out by Bowden[3] for a NACA 0011 airfoil with a deicing boot. Bowden[3] also showed how the lift coefficient decreased as ice was accreted between deicer operations and then how the lift increased when the boot was operated and the ice shed. While these results provided important insight into the performance effects of residual and intercycle ice accretions, a major shortcoming was that the data were acquired at fixed angle of attack. Therefore, the airfoil stall characteristics with these ice accretions was not documented.

The effect of intercycle ice accretions on airfoil stalling characteristics was investigated as part of a larger study by Jackson and Bragg.[4] Intercycle ice-shape tracings were recorded during tests on a 48-inch chord NLF 0414 airfoil model for one icing cloud condition. Two-dimensional (i.e., no spanwise variation) ice-shape simulations were produced from ice tracings and attached to the leading edge of an 18-inch chord NLF 0414 airfoil model. The performance degradation in maximum lift was on the order of 30%. However, the effect of the three-dimensional characteristics of the intercycle ice accretions was not documented.

A more recent investigation using high-fidelity simulations of intercycle ice accretions showed significant airfoil performance degradations. Broeren, Addy and Bragg[5] generated intercycle ice accretions on a 36-inch chord NACA 23012 airfoil model equipped with pneumatic deicing boots. Molds were made of selected intercycle ice accretions that were later used to produce castings that were attached to the leading edge of a 36-inch chord NACA 23012 airfoil model used for aerodynamic testing. The aerodynamic testing was performed in a pressure tunnel where the Reynolds was varied from 2.0×10^6 to 10.5×10^6 and the Mach number was varied from 0.10 to 0.28. Typical results showed that the intercycle ice accretions resulted in a 60% decrease in maximum lift. The authors suggested that this large performance penalty was related to the ridge-like features of the intercycle accretions and the sensitivity of the NACA 23012 airfoil to this type of ice shape.

Studies by Lee[6] and Lee *et al.*[7-9] have shown that the clean airfoil geometry (i.e., pressure distribution) can influence the aerodynamic severity of a spanwise-ridge ice accretion. These studies were carried out using a forward-facing quarter-round shape with normalized height (k/c) of 0.0139. The quarter-round was uniform in size and shape across the model span and was positioned at several different chordwise locations. Two of the airfoils tested with this simulated ice ridge were the NACA 23012m and the NLF 0414. The NACA 23012m was a slightly modified version of the standard NACA 23012 and it had a 25% chord simple flap. The NLF 0414 airfoil also had a 25% chord simple flap. Some key results are summarized in Reference 8. The lowest $C_{l,max}$ on the NACA 23012 airfoil was 0.25 with the quarter-round located near x/c = 0.12. In contrast, the lowest $C_{l,max}$ on the NLF 0414 was 0.68 and this did not vary significantly with ice-shape location between x/c = 0.02 and x/c = 0.20. The reason given for this difference was that the large leading-edge suction pressures on the clean NACA 23012 airfoil were prevented from forming in the iced case, thus resulting in the large lift reductions. The clean NLF-0414 had a relatively uniform chordwise pressure loading and this was not as significantly affected by the ice shape, thus resulting in the smaller lift reductions.

The purpose of this paper is to demonstrate how the performance of three different airfoils was affected by the same intercycle ice-accretion simulation. The airfoils considered were the NACA 23012, NACA 3415 and the NLF 0414. These have pressure distributions and geometries that are quite different. The intercycle ice shapes used in this investigation were adapted from those presented in Reference 5. The ice-shape simulations were built up on the airfoil models using various sizes of grit roughness. Performance data were then acquired over a large angle of attack range, including stall at a Reynolds number of 1.8×10^6 and a Mach number of 0.18.

Experimental Arrangement

All of the aerodynamic testing was carried out at the University of Illinois Subsonic Aerodynamics Laboratory using the low-speed, low-turbulence wind tunnel. This wind tunnel was of open-return type with a 3-ft by 4-ft rectangular working section and the maximum speed was approximately 235 ft/sec. The airfoil models all had a 1.5-ft chord and spanned the 3-ft height of the test section. The NACA 23012 airfoil was a single element model, while the NACA 3415 and NLF 0414 airfoils each had a 25% chord simple flap. The airfoil cross-sections are shown in Fig. 1. The flap

geometries have been eliminated from the figure for clarity. The NACA 3415 airfoil was the thickest (t/c = 0.15) followed by the NLF 0414 (t/c = 0.14) and the NACA 23012 (t/c = 0.12).

The airfoil models were supported by a three-component force balance located below the test-section. The schematic drawing in Fig. 2 shows this arrangement for one of the flapped models. The flap position was controlled by a two-member linkage system driven by a linear traverse. The traverse was mounted to the metric force plate of the balance. For the present series of tests, the flap angle was fixed at zero degrees and the flap gap was sealed on the lower surface. All of the models had a dense distribution of pressure taps located in a main chordwise row near the midspan location and a secondary spanwise row. Also shown in Fig. 2 is the traversable wake rake used to obtain the airfoil drag. Both the wake pressures and model surface pressures were measured with an electronically scanned pressure (ESP) system. More details about this experimental arrangement can be found in Lee.[6]

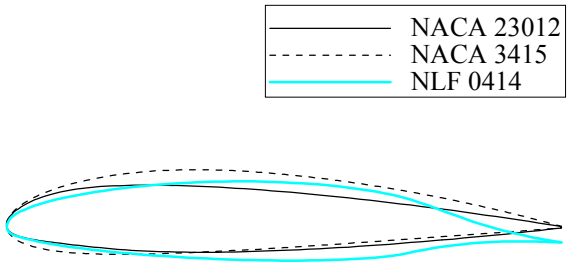

Fig. 1 The airfoils tested in this study (flap geometry omitted for clarity).

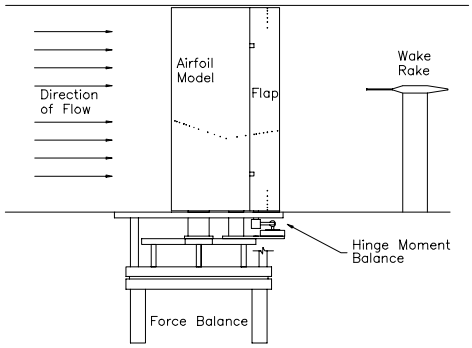

Fig. 2 Schematic drawing of experimental apparatus, after Lee.[6]

The lift coefficient (C_l) and pitching-moment coefficient (C_m) taken about the quarter-chord were derived from both the force balance and the surface-pressure measurements. The agreement in the results from these two methods was very good. In this paper only the values from the pressure measurements are shown for simplicity. The drag coefficient (C_d) was calculated from the wake pressures using standard momentum-deficit methods. All of these aerodynamic coefficients and the angle of attack were corrected for wall interference effects using the methods of Rae and Pope.[10] The experimental uncertainty in these coefficients was also estimated using the methods of Kline and McClintock[11] and Coleman and Steele[12] for 20:1 odds. Table 1 lists these uncertainties for a set of pressure-derived coefficients, except for the angle of attack, which was obtained directly from the force balance. The values were determined by Lee[6] and Lee and Bragg[9] for free-steam conditions of $Re = 1.8\times10^6$, $Ma = 0.18$. The relative uncertainty in C_m seems large for this example owing to the small reference value. For cases where the C_m values were larger, the absolute uncertainty would be similar, therefore resulting in a lower relative uncertainty.

Table 1 Estimated Experimental Uncertainties

Aerodynamic Quantity	Reference Value	Absolute Uncertainty	Relative Uncertainty
α	5.00	±0.02	±0.40%
C_p	-0.712	±0.0037	±0.52%
C_l	0.633	±0.00211	±0.33%
C_m	-0.0089	±0.000349	±3.90%
C_d	0.0102	±0.000143	±1.40%

The intercycle ice-accretion simulations tested on the three airfoils were adapted from those recorded and presented in References 5 and 13. In that work, four accretions were selected for testing in the NASA Langley LTPT. They were designated by the numbers 290, 296, 312 and 322, after the icing run number. Tracings for each shape are shown in Fig. 3. The ice-shape castings used for the LTPT experiments in references 5 and 13 represented the highest-fidelity simulation since the ice accretions had very irregular roughness sizes and spanwise variation. Despite this, a common characteristic among the ice shapes were ridge-like features that were distinct formations in the roughness. Both the ice accretion and aerodynamic tests were carried out using a 36-inch chord NACA 23012 airfoil. Therefore, the simulations were scaled down by a factor of 2 when simulated on the 18-inch chord models used in the present investigation. The relative chordwise locations of ice-shape features (such

as characteristic ridges) were also preserved for these experiments. For example, an ice feature located at *x/c* = 0.04 would be maintained for each airfoil, even though the distance measured along the surface would be slightly different. The authors concede that the character of the ice accretions may be different if accreted on each of the three airfoils separately. However, this did not compromise the main objective of this study which was to determine the effect of airfoil geometry on the performance degradation. In fact, to determine the effect of airfoil geometry on the aerodynamics with intercycle ice, the same ice simulation must be tested on each airfoil.

The intercycle ice simulations for the present experiments were constructed from various sizes of loose grit roughness. This material was useful for representing the surface irregularities of the actual ice accretions. These roughnesses were applied to the models using a substrate of double-sided tape. The chordwise distribution of ice thickness was controlled by using roughness of different sizes. Ridge-like features were built-up at the appropriate chordwise location by layering the roughness. A spray adhesive was used to hold the roughness in place. Spanwise variation was also incorporated into the simulations, but with less fidelity as the chordwise variations. Figure 4

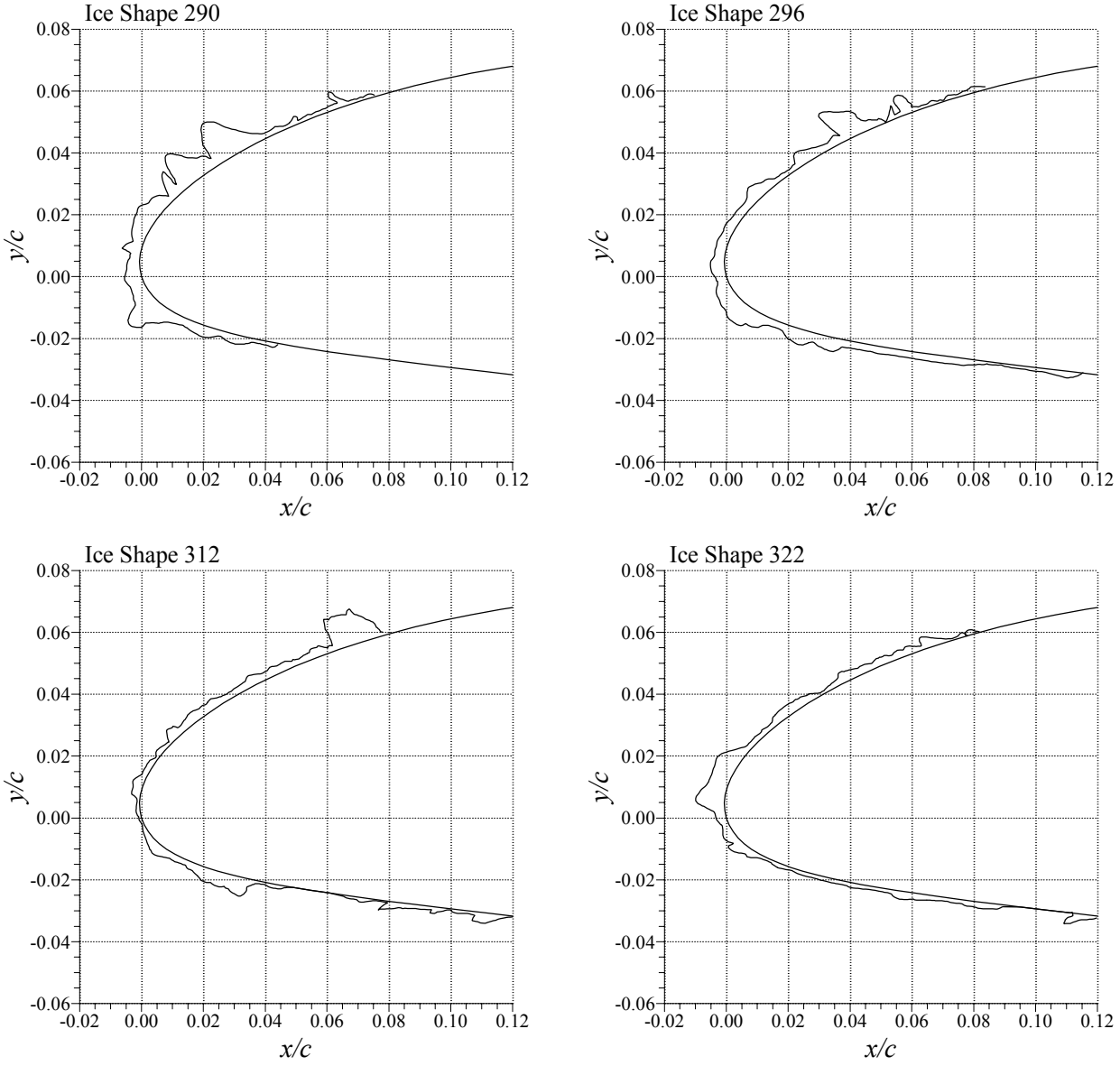

Fig. 3 Tracings of the four intercycle ice accretions that were simulated in this study, after Ref. 5, 13.

shows a comparison of an actual ice shape (on a 36-inch chord model) with the roughness simulation (on an 18-inch chord model). The figure also shows how the ice-shape simulation was place on either side of the pressure tap row so that the approximate pressure distribution could be measured. The lift and pitching moment determined from integration of the pressure distribution agreed very well with the force-balance data.

In addition to the intercycle ice simulations, the airfoil models were also tested with standard roughness in the form of 80- and 150-grit paper-backed garnet sandpaper. The purpose of these tests was to provide a very repeatable form of simulated ice roughness that could be identically duplicated on each of the airfoil models. As shown in Table 2, these grit sizes approximately represented the chord-length scaled equivalent of the 40- and 80-grit sizes that were tested in the LTPT.[5,13] The roughness heights listed in the table do not include the thickness of the paper backing that was approximately one and a half times as large as the roughness itself. Also, 0.003-inch thick double-sided tape was used to attach the sandpaper to the model. The surface extent of the sandpaper roughness was x/c = 0.010 on the lower surface to x/c = 0.07 on the upper surface and was cut out around the pressure orifices.

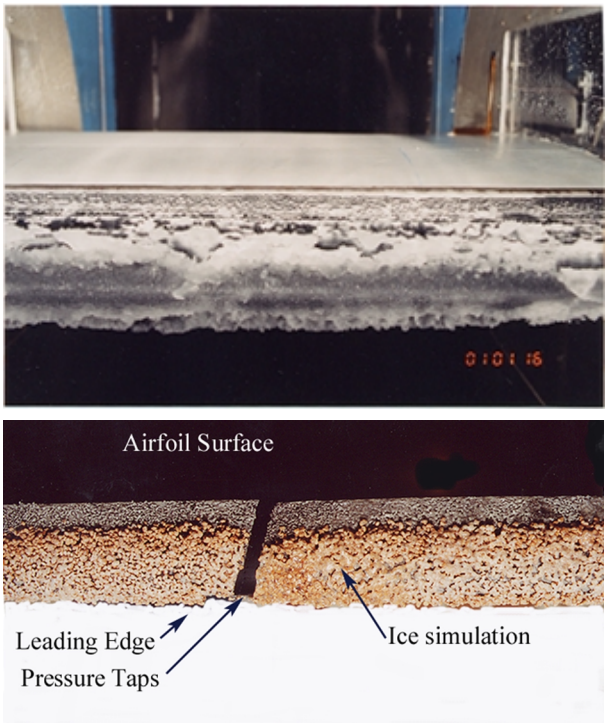

Fig. 4 Comparison between ice shape 290 (top) with the roughness simulation.

Table 2 Comparison of Sandpaper Roughness Heights

Sandpaper Grit Number	Roughness Height* (k, in.)	Normalized Height (k/c) for c = 36 in.	Normalized Height (k/c) for c = 18 in.
40	0.0205	0.00057	0.00114
80	0.0083	0.00023	0.00046
150	0.0041	0.00011	0.00023

*based on nominal size of commercial carborundum[10]

Results

Clean Airfoil Results

The three airfoils tested in this study were selected because their clean aerodynamic characteristics were substantially different. This is illustrated in the performance plot of Fig. 5 for data acquired at Re = 1.8×10^6 and Ma = 0.18. The lift data show that the NACA 23012 airfoil had the highest $C_{l,max}$ of about 1.47. This was followed by the NACA 3415 ($C_{l,max}$ = 1.37) and the NLF 0414 ($C_{l,max}$ = 1.34). The lift curve for the NLF 0414 airfoil exhibited a distinct change in slope near α = 2 deg. This resulted from trailing-edge separation aft of about x/c = 0.70 on the airfoil upper surface. The pitching-moment data show that the NACA 23012 had the lowest values, followed by the NACA 3415 and then the NLF 0414 airfoil. This indicated that the NACA 23012 had the least amount of positive camber. The NLF 0414 had the lowest drag in the range of $-3 < \alpha < 3$ deg., since it was a laminar flow airfoil. For angles of attack greater than 3 deg. there was significant flow separation at this Reynolds number aft of about x/c = 0.70 on the upper surface, which resulted in higher drag than the two NACA airfoils.

The differences in these airfoils are even more evident in the pressures distributions. An example is shown in Fig. 6 for a similar, nominal lift coefficient of 0.6. This corresponded to different angles of attack for each airfoil as indicated by Fig. 5. The pressure distributions for the NACA 3415 and NLF 0414 airfoils show the expected discontinuities near x/c = 0.75 due to the flap gap. The NACA 23012 airfoil had a very large suction peak (with $C_{p,min}$ = –1.6) centered near x/c = 0.06. There was a severe pressure recovery (with very large adverse pressure gradient) from x/c = 0.08 to 0.22. The pressure recovery was more gradual downstream of this location and extended to the trailing edge. The NACA 3415 airfoil had a pressure distribution that was quite different. A large suction peak was not present on this airfoil at this angle of attack, with a $C_{p,min}$ value of –1.2 located near x/c = 0.18. The pressure recovery here was more gradual since a large suction peak was

not present. The pressure gradient was nearly constant from x/c = 0.25 to the trailing edge. The NLF 0414 airfoil had a nearly constant suction pressure between x/c = 0.04 to x/c = 0.72. Downstream of this location, there was a very severe adverse gradient that led to the trailing-edge flow separation describe above.

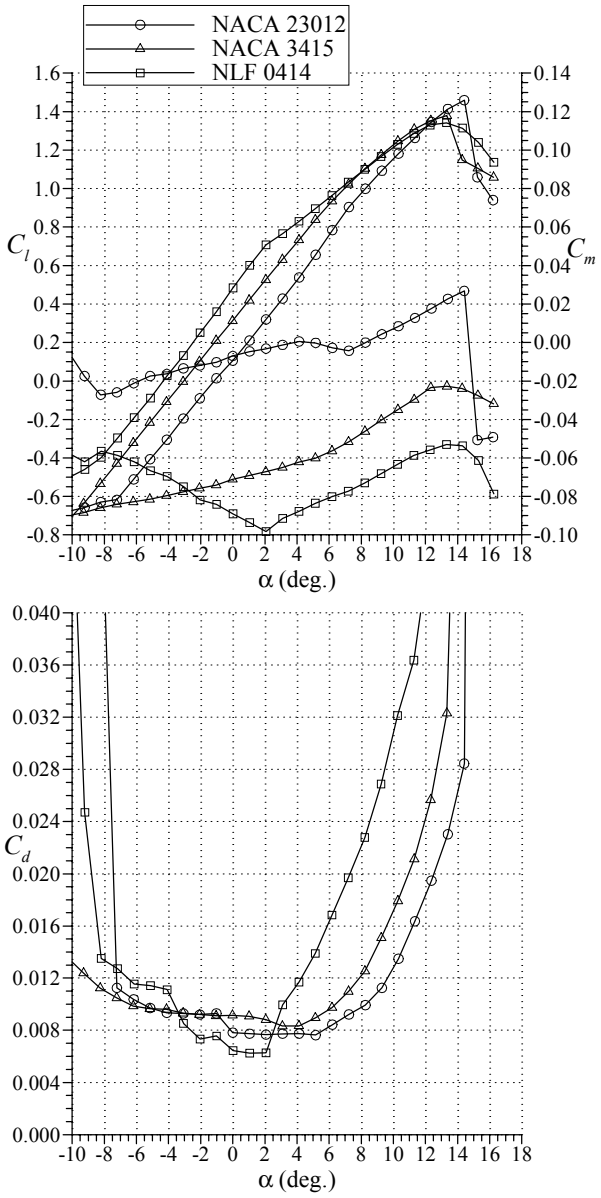

Fig. 5 Comparison of the clean airfoil performance at $Re = 1.8\times10^6$, $Ma = 0.18$.

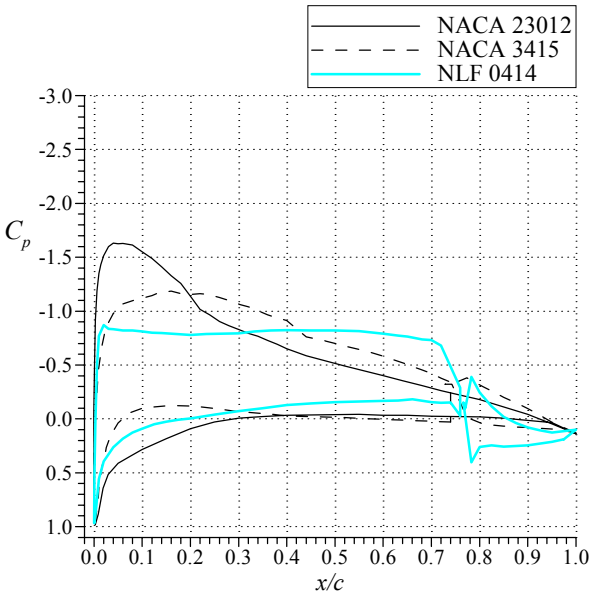

Fig. 6 Comparison of clean airfoil pressure distributions at approximately matched $C_l = 0.6$.

The NACA 23012 airfoil was tested in the clean configuration by Broeren *et al.*[5,13] in the Low-Turbulence Pressure Tunnel (LTPT) at NASA Langley and at the University of Illinois for the present tests. These results are plotted in Fig. 7 for closely match Reynolds and Mach number conditions. The data show good agreement in the lift-curve until the maximum lift region where the LTPT data had a slightly higher $C_{l,max}$ value. This discrepancy is small and may even have been attributable to the small difference in Reynolds number. The present pitching-moment data were slightly more nonlinear. Agreement in the drag values are good except at certain odd angles of attack (e.g., -1 and 5 deg). Comparison here is difficult because there were no wake-survey drag data available in the LTPT data set for odd numbered angles of attack. Despite these minor discrepancies, the cross-facility comparisons are reasonable.

Iced-Airfoil Results for the NACA 23012 Airfoil

The effect of the intercycle ice shapes on the performance of the NACA 23012 airfoil was thoroughly discussed in References 5 and 13. Some of that data are shown again here in order to validate the accuracy of the built-up roughness simulations used for the present series of tests. The LTPT data were acquired using castings of the ice shapes and this was considered to be the most reliable method of simulation. The performance data are summarized in Fig. 8, for $Re = 2.0\times10^6$ and $Ma = 0.10$ (except for the clean data at $Re = 2.0\times10^6$ and $Ma = 0.21$). The intercycle ice shapes resulted in large performance

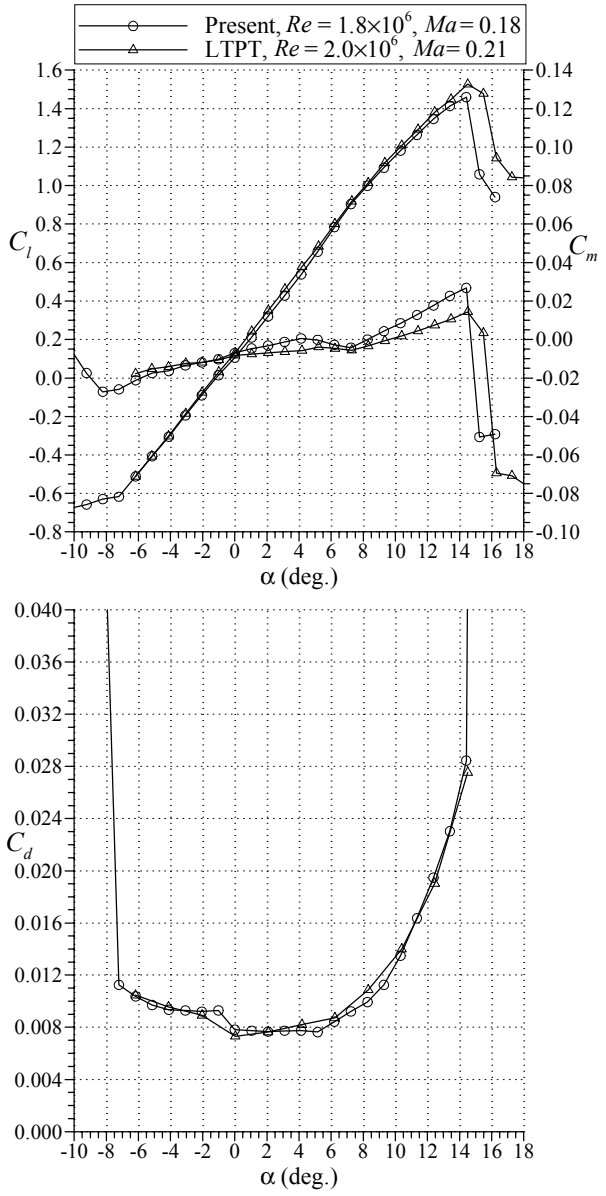

Fig. 7 Comparison of the present NACA 23012 airfoil performance data with LTPT results from Broeren *et al.*[5,13]

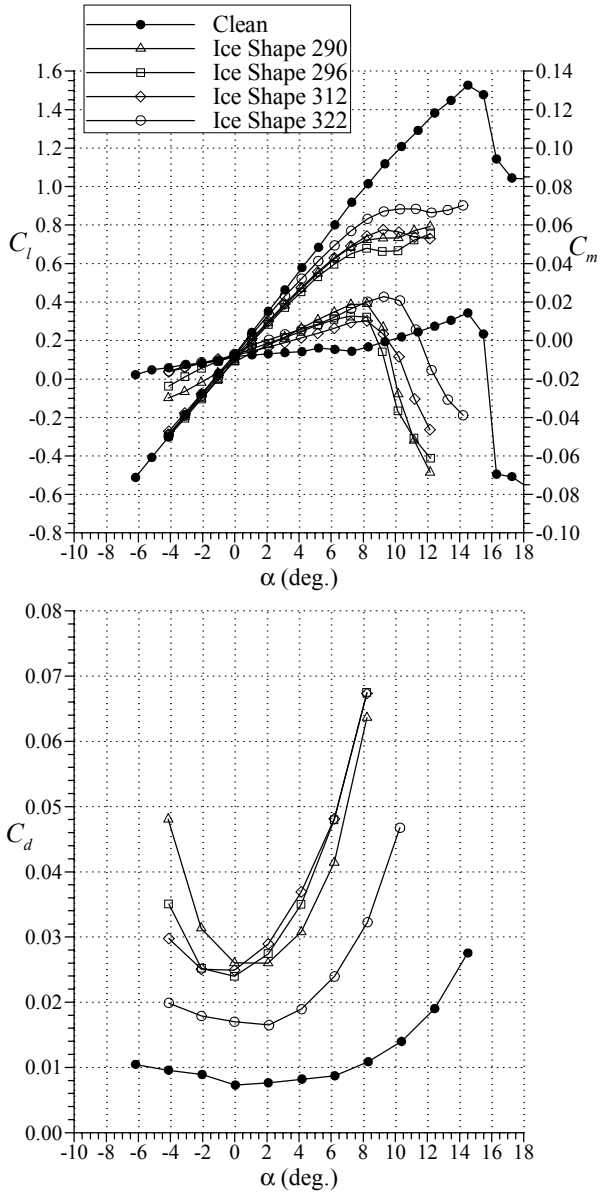

Fig. 8 Effect of intercycle ice-casting simulations on NACA 23012 airfoil performance. LTPT data after Broeren *et al.*[5,13] (Clean data at $Re = 2.0\times10^6$, $Ma = 0.21$; iced data at $Re = 2.0\times10^6$, $Ma = 0.10$)

penalties, especially in terms of maximum lift degradation. Three of the four intercycle shapes caused $C_{l,max}$ values in the range of 0.65 to 0.78 and stall angles in the range of 8 to 10 deg. The remaining ice shape 322 had a slightly higher $C_{l,max}$ value of about 0.90. The intercycle shapes produced a stronger angle of attack dependence in the pitching moment. The minimum drag values for three of the four shapes was a three-fold increase from the clean case. The airfoil with ice shape 322 had a lower drag than the others, likely because this ice shape was smaller and smoother.

These ice shapes were simulated at half-scale and were tested at Illinois. These data are shown in Fig. 9 for $Re = 1.8\times10^6$ and $Ma = 0.18$. The performance data here were very similar to the results in Fig. 8. The maximum lift coefficient for three of the four ice shapes was in the range of 0.65 to 0.80, with ice shape 322 resulting in a $C_{l,max}$ of 0.90. The stalling angles of attack were reduced to 7 to 9 deg., except for ice shape 322 which had an α_{stall} closer to 10 deg. An iced-airfoil $C_{l,max}$ value of 0.70, amounted to a 52% reduction from the clean value of 1.47. The pitching moment data in

Fig. 9 mimic the angle of attack dependence exhibited in Fig. 8. The most variation in the results from the half-scale intercycle ice simulations was in the drag data. The drag values for the airfoil with the ice-shape 290 simulation tested at Illinois was higher than the ice-shape casting tested at LTPT. On the other hand, the drag values for ice shape 312 were slightly lower for the half-scale simulation. However, given the random nature of the ice-shape features and the spanwise variation in drag, this comparison in the drag values could be considered quite good.

A detailed comparison of the performance data is shown in Fig. 10 for two of the four intercycle ice shapes. Here again the lift data show that the half-scale simulations were very effective in reproducing the lift-performance degradations caused by the high-fidelity castings tested at LTPT. Agreement in the pitching-moment data was not as good, but the general trends

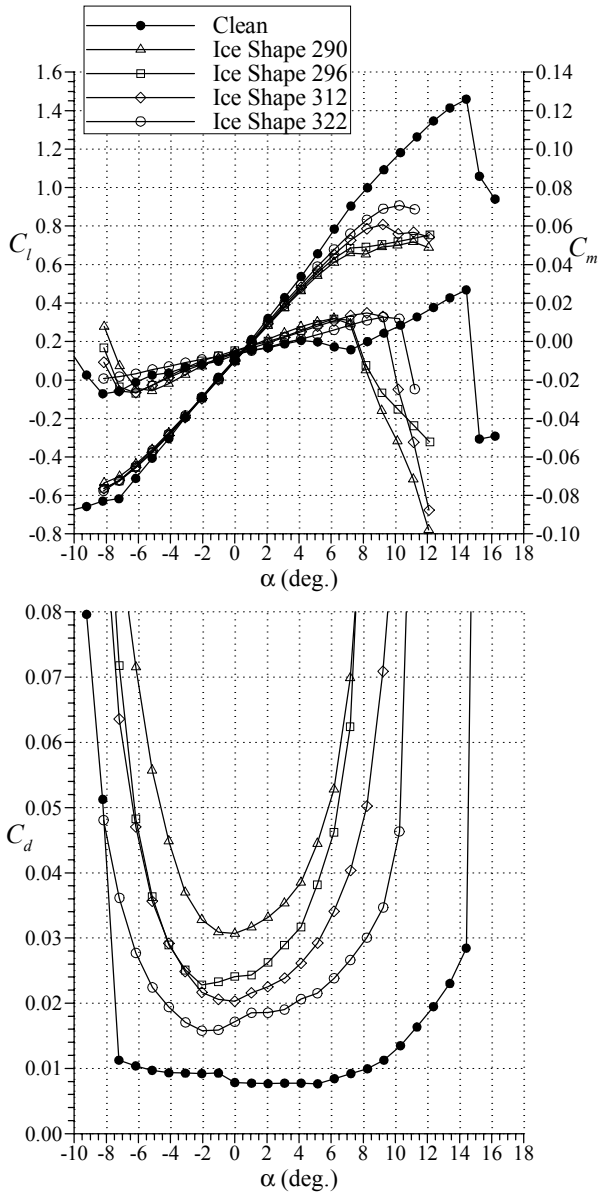

Fig. 9 Effect of intercycle ice simulations on NACA 23012 airfoil performance, data from the present study, at $Re = 1.8\times10^6$, $Ma = 0.18$.

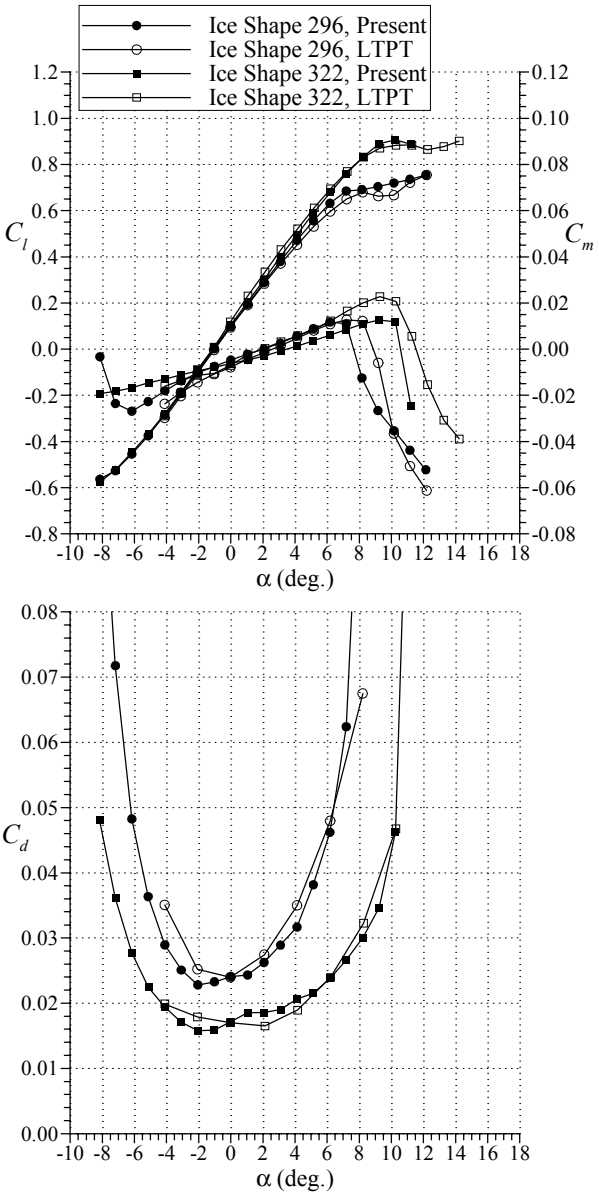

Fig. 10 Comparison of present and LTPT performance data for the NACA 23012 with simulated intercycle ice shapes. Present data at $Re = 1.8\times10^6$, $Ma = 0.18$ and LTPT data at $Re = 2.0\times10^6$, $Ma = 0.10$, after Broeren *et al.*[5,13]

were certainly represented in the present data. The agreement in the drag values was reasonable. These data, taken as a whole indicate that the methods used to simulate the intercycle shapes on the 18-inch chord models were valid. The data also imply that a simple geometric scaling is appropriate for ice features of this type and size.

In addition to the intercycle ice-shape simulation tests, standard roughness was also applied to the airfoil leading edge. For tests on the 36-inch chord LTPT model, 40- and 80-grit sandpaper was used. The geometrically scaled equivalent sized sandpaper for the 18-inch chord model used for the present tests was nominally 80- and 150-grit. The performance effects of this uniform roughness are summarized in Fig. 11 for the NACA 23012 airfoil at $Re = 1.8\times10^6$ and $Ma = 0.18$. The data show that the lift degradation caused by the uniform roughness was very significant with $C_{l,max}$ values near 1.10. However, these were substantially higher maximum lift values than for the airfoil with the intercycle ice simulations. Also noteworthy is the fact that there was very little difference in the lift performance between the 80- and 150-grit sandpaper, despite the almost two-fold difference in roughness height. The effect of the uniform roughness on the pitching moment was similar to that caused by the ice-shape simulations. The drag values were increased from the clean case by less than a factor of two in the linear range of the lift curve.

The geometric size scaling of the sandpaper roughness height was also validated by comparison with the LTPT data in References 5 and 13. These results are given in Fig. 12 for the 40/80-grit case. The maximum lift values from both tests were nearly identical, while the stalling angle of attack was one degree lower for the present data. This angle of attack discrepancy is small and could be less than one degree if the data were acquired in smaller increments. Agreement in the pitching moment variation with angle of attack was not quite as good between the two tests. Similarly, agreement in the measured drag values was very good, except over the range of $-2 < \alpha < 4$ deg. Despite these small discrepancies the data show that the geometric scaling of the roughness height was also appropriate for this case.

Iced-Airfoil Results for the NLF 0414 and NACA 3415

The intercycle ice-shape simulations were tested on the NLF 0414 and NACA 3415 airfoils to gauge their sensitivity to this class of ice shape. Significant degradations in performance were also observed. The results for the NLF 0414 airfoil are shown in Fig. 13. The stall behavior with the ice simulations was similar to the NACA 23012 data in that there was a large range of $C_{l,max}$ from 0.90 to 1.05. The same ice shape 322 also resulted in the highest $C_{l,max}$. These iced-airfoil lift coefficients were significantly higher than the range for the ice simulations on the NACA 23012 airfoil which was 0.65 to 0.90. For example, an iced airfoil $C_{l,max}$ value of 0.95, constituted a 29% reduction from the clean value of 1.34. This is consistent with that reported by Jackson and Bragg[4] for other intercycle ice simulations tested on the NLF 0414 airfoil. This value is nearly half that of the 52% reduction in maximum lift observed for the NACA 23012 airfoil.

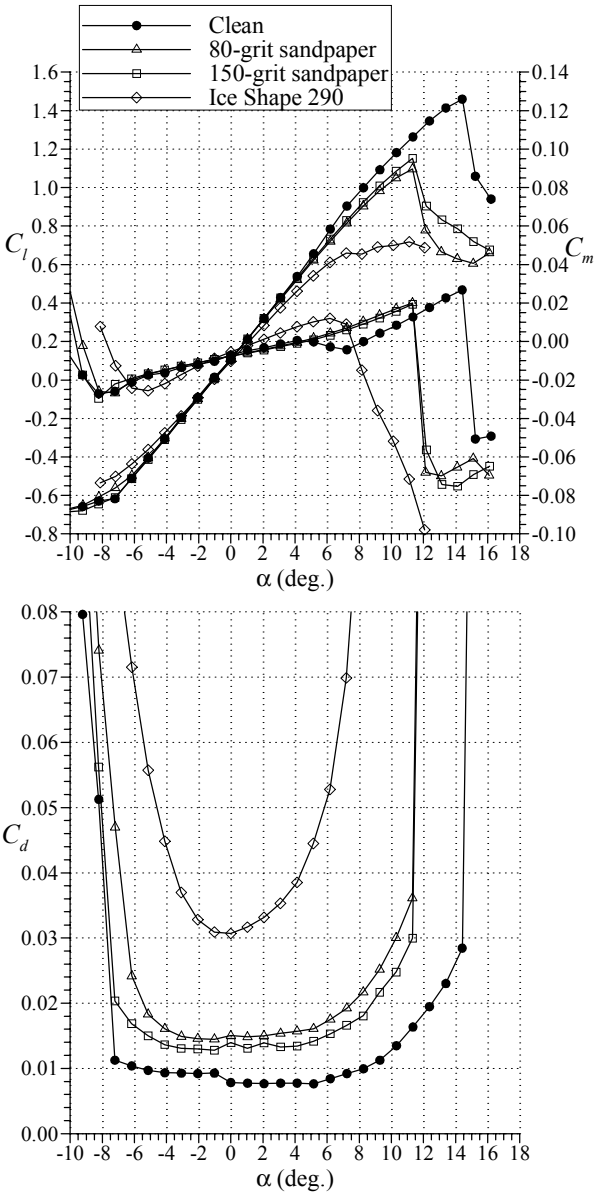

Fig. 11 Effect of 80- and 150-grit sandpaper roughness on NACA 23012 airfoil performance, data from the present study at $Re = 1.8\times10^6$, $Ma = 0.18$.

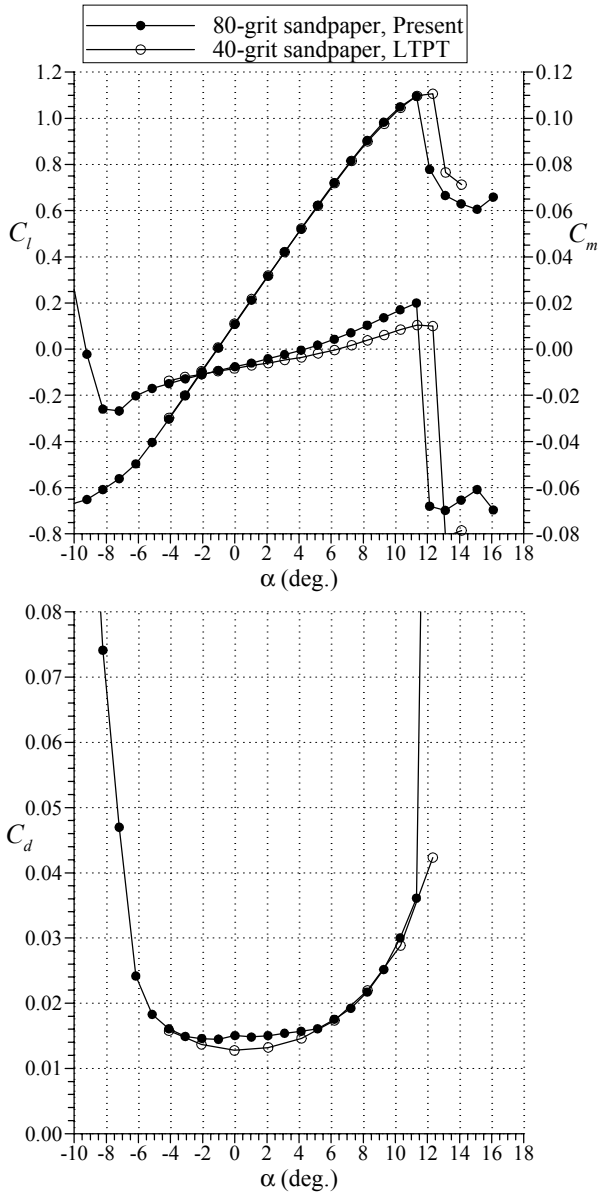

Fig. 12 Comparison of present and LTPT performance data for the NACA 23012 with sandpaper roughness. Present data at $Re = 1.8\times10^6$, $Ma = 0.18$ and LTPT data at $Re = 2.0\times10^6$, $Ma = 0.10$, after Broeren *et al.*[5,13]

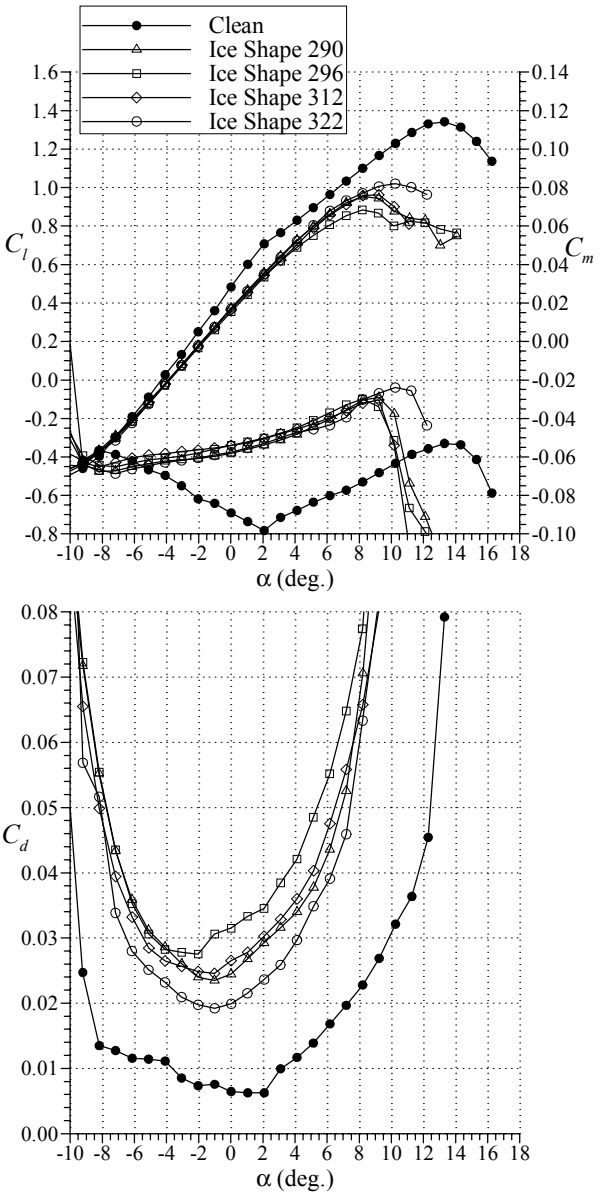

Fig. 13 Effect of intercycle ice simulations on NLF 0414 airfoil performance at $Re = 1.8\times10^6$, $Ma = 0.18$.

A key difference in lift performance with the ice simulations between the two airfoils was observed for lift coefficients in the range of 0.0 to 0.6. In this range, the simulated ice had a more severe effect for the NLF 0414 airfoil than for the NACA 23012, as there were larger differences between the clean and iced lift coefficients. The effect of the simulated ice on the NLF 0414 airfoil pitching moment and drag were also similar to the effects on the NACA 23012 airfoil performance.

The performance of the NACA 3415 airfoil with the intercycle ice simulations was similar to the NLF 0414 airfoil as depicted in Fig. 14. In this case, there was less variation in maximum lift coefficient with the different ice shapes. The $C_{l,max}$ values ranged from about 0.85 to 0.95. An iced-airfoil $C_{l,max}$ of 0.90 constituted a 34% reduction from the clean value of 1.37. This reduction is more similar to the NLF 0414 airfoil performance than for the NACA 23012 with the same simulated ice shapes. The lift penalties caused by

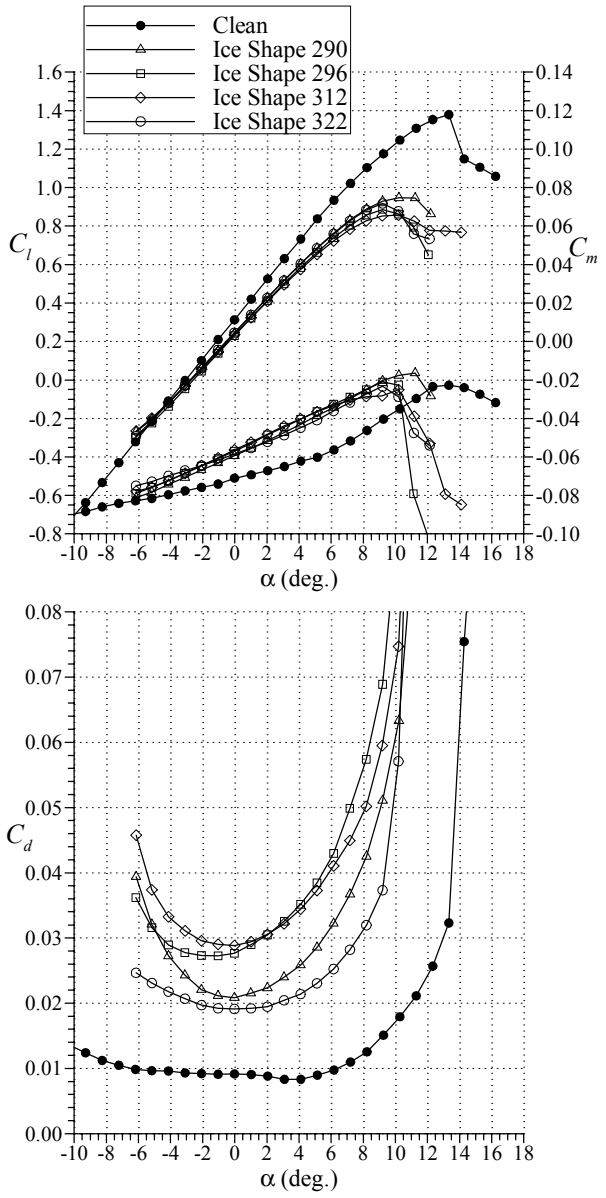

Fig. 14 Effect of intercycle ice simulations on NACA 3415 airfoil performance at $Re = 1.8\times10^6$, $Ma = 0.18$.

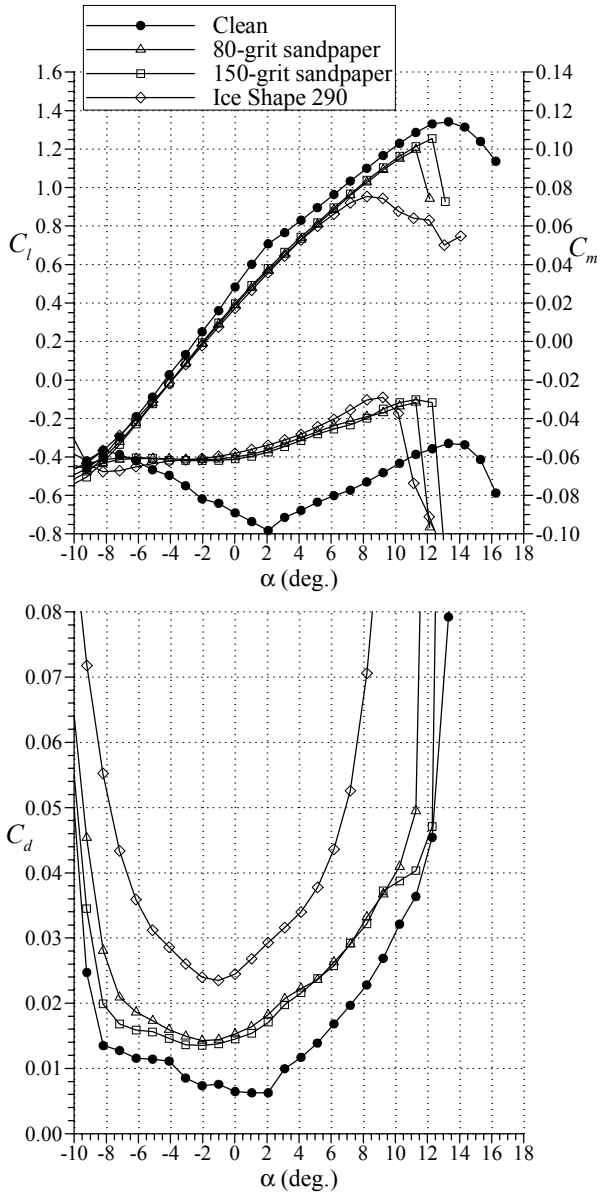

Fig. 15 Effect of 80- and 150-grit sandpaper roughness on NLF 0414 airfoil performance at $Re = 1.8\times10^6$, $Ma = 0.18$.

the ice shapes for the NACA 3415 airfoil were very similar to the NLF 0414 airfoil in the range of $C_l = 0.0$ to 0.6. The effects on pitching moment and drag were also similar to the other airfoils.

The NLF 0414 and NACA 3415 airfoils were also tested with the uniform roughness applied to the leading edge of the airfoils. Results for the NLF 0414 airfoil are shown in Fig. 15. As with the intercycle ice simulations, the sandpaper roughness caused significantly smaller reductions in maximum lift from the clean value for this airfoil as compared to the NACA 23012 airfoil. However, the roughness altered the stalling characteristics such that there was a significant drop in lift beyond $C_{l,max}$. This change in stall behavior from the clean case with the roughness present was not observed for the other two airfoils. The performance effects of the various intercycle ice shapes and standard roughness on the three airfoils is discussed in more detail below.

Discussion

Airfoil and Ice-Shape Geometry Effects

The effect of the intercycle ice simulations on maximum lift is summarized in Fig. 16 for the three airfoils tested. The chart reiterates the preceding results that these ice shapes had the most severe effect, in terms of maximum lift degradation, for the NACA 23012 airfoil. On the other hand, the maximum lift values for the NLF 0414 airfoil were least affected by the intercycle ice shapes. The NACA 3415 airfoil results were similar to the NLF 0414 data for ice shapes 290 and 296. For the remaining two ice shapes, the NACA 3415 $C_{l,max}$ values were between the NACA 23012 and NLF 0414 results. The uniform roughness results were somewhat more mixed, given that the NACA 3415 airfoil had the lowest $C_{l,max}$ values for each case. These values were very comparable to the NACA 23012 airfoil results and both were substantially less than the NLF 0414 airfoil with standard roughness.

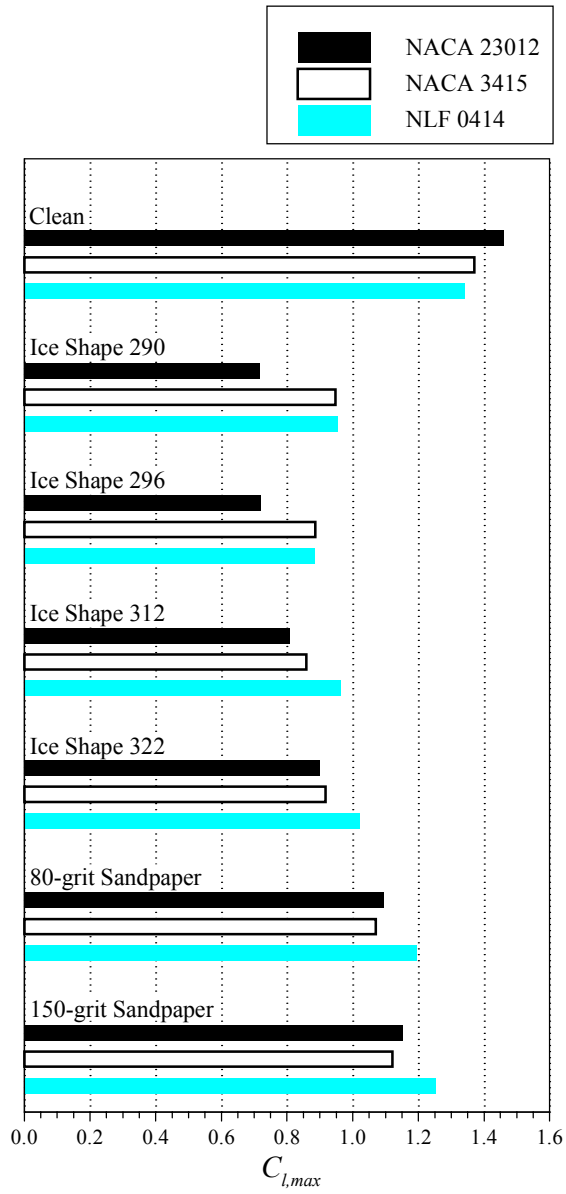

Fig. 16 Summary of intercycle ice simulations and sandpaper roughness effect on maximum lift for the three airfoils tested.

The large reductions in maximum lift caused by the intercycle ice accretions on the NACA 23012 was likely related to the pressure distribution on the clean airfoil. Since the clean NACA 23012 airfoil had large suction pressures near the leading edge, even for moderate lift coefficients, the airfoil was particularly sensitive to protuberances in this region. This effect is illustrated in Fig. 17 which compares the clean and iced pressure distributions on the NACA 23012 airfoil. The data are for $\alpha \approx 8.3$ deg. which was close to maximum lift for the airfoil with ice shape 296. The plot shows how the ice shape reduced the suction pressures on the upper surface over the first 20% of the chord. There was also significant deviation of the lower-surface pressures. This is contrasted with the effect of the uniformly distributed roughness shown in Fig. 18. The data are for $\alpha \approx 11.4$ deg. which was close to the maximum lift for the NACA 23012 airfoil with the 80-grit sandpaper over the leading edge. The pressure distribution shows that there was significant deviations only in the region of the minimum pressure peak.

This contrast between the effect of the intercycle ice shapes versus the uniform roughness was observed for all of the airfoils tested. A side-by-side comparison of the intercycle ice accretions and the sandpaper roughness reveals that their geometries were quite different. The sandpaper had a very uniform array of roughness, whereas the intercycle ice accretions contained ridge-like features that were not uniform, especially in the spanwise direction. Another factor was that even the larger uniform roughness (80-grit) was considerably smaller in size than the actual accretions. For example, the nominal height (ignoring the larger ridge-like features) of ice shape 296 was on the order of $k/c = 0.0050$ (cf. Fig. 3). This was more than a factor of ten larger than the height of the 80-grit sandpaper at $k/c = 0.00046$ (cf. Table 2). These results tend to support the conclusions of Shin and Bond[1] that uniform roughness may not be an adequate method for simulating intercycle ice. However, the present study did not consider uniform roughness that was appropriately sized to the nominal height of the intercycle accretions.

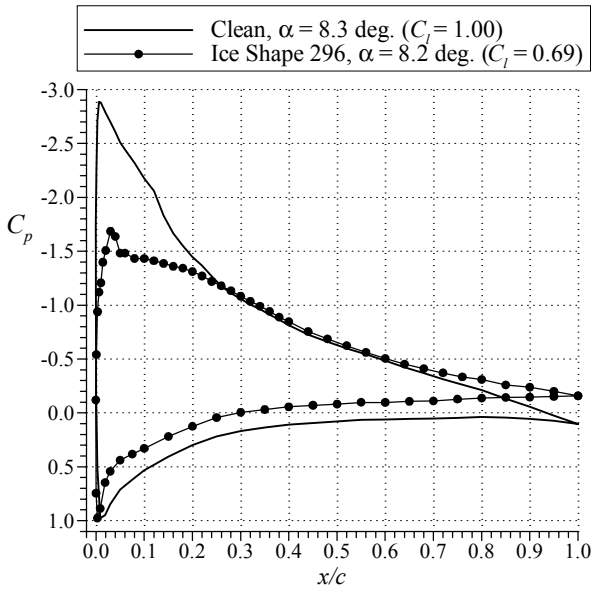

Fig. 17 Comparison of clean and iced pressure distributions for the NACA 23012 airfoil at matched angle of attack near stall in the iced configuration.

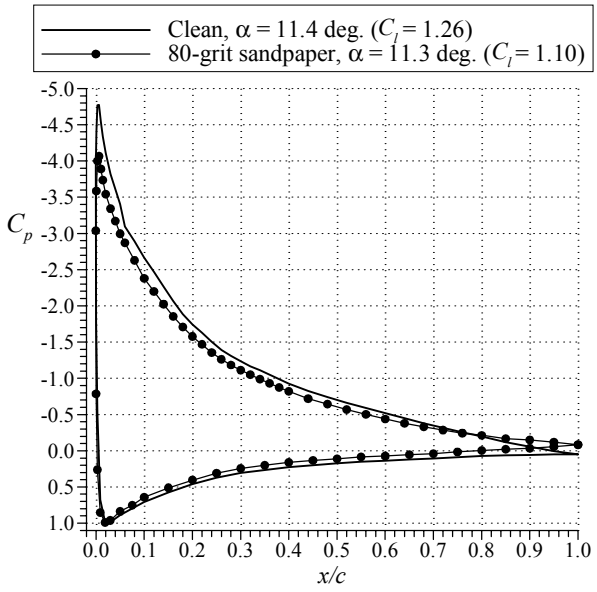

Fig. 18 Comparison of clean and sandpaper roughness pressure distributions for the NACA 23012 airfoil at matched angle of attack near stall in the sandpaper roughness configuration.

The ridge-like features of the intercycle ice shapes likely played a strong role in the resulting performance degradation. The sensitivity of the NACA 23012 airfoil to ridge-type protuberances was investigated by Lee[6] and Lee *et al.*[7-9] using forward-facing quarter-rounds having heights of k/c = 0.0083 to 0.0139. The authors found that the maximum lift decreased significantly as the quarter-round was located from the leading downstream to about x/c = 0.12. Broeren *et al.*[5] noted that the ridge-like features present in the intercycle ice accretions were found to vary in height from k/c = 0.0091 to 0.0138 and the location on the airfoil surface varied from x/c = 0.00 to 0.06. A detailed comparison with the data of Lee[6] and Lee *et al.*[6-8] showed similar trends, but that the intercycle ice accretions had a less severe effect on maximum lift. This was attributed to the spanwise breaks or gaps in the intercycle accretions that were not present in the quarter-round testing.

It was noted above that the intercycle ice simulations resulted in more severe lift penalties for the NACA 3415 and NLF 0414 airfoils in the range of C_l = 0.0 to 0.6. This effect is illustrated in Figs. 19 and 20. The pressure distributions are plotted for the NACA 23012 and the NLF 0414 airfoils at a clean $C_l \approx 0.5$ and with the ice shape 296 simulation at the same angle of attack. For the NACA 23012 airfoil (Fig. 19), the ice simulation did not significantly alter the clean pressure distribution. The iced-airfoil lift coefficient of 0.47 was slightly reduced from the clean value of 0.54. There was a higher suction peak owing to the local flow acceleration around the ice roughness. This was followed by a more severe adverse pressure gradient up to $x/c \approx 0.25$, where the clean and iced pressure distributions were very similar. There was some small divergence of the trailing-edge pressure that was perhaps indicative of boundary-layer separation. In the case of the NLF 0414 airfoil (Fig. 20), small suction peaks caused by the ice shape were evident on both the upper and lower surface. This resulted in significantly lower suction pressures on the upper surface from $x/c \approx$ 0.15 to 0.75. In this case the iced-airfoil C_l was 0.35 compared to the clean value of 0.48 for the same angle of attack. Very similar results were observed for the NACA 3415 airfoil. Therefore, the lift of airfoils having a more uniform pressure loading may have a greater sensitivity to this type of ice accretion than forward-loaded sections like the NACA 23012 over the range of low to moderate lift coefficients.

It is also noteworthy that this effect on the iced-airfoil pressure distribution continues for higher lift coefficients leading up to the stall. This trend is illustrated in Fig. 21 for the NACA 3415 airfoil at $\alpha \approx 8$ deg. This angle of attack is very close to maximum lift for the airfoil with the ice shape 296 simulation. The trend here is analogous to that in Fig. 20 for the NLF 0414 airfoil at lower lift coefficient. The suction peak with the ice shape present is reduced somewhat, but the upper surface suction pressures are lower than in the clean case from $x/c \approx 0.12$ to 0.75. Contrast this with the NACA 23012 results shown in Fig. 17, where the

suction pressures were reduced only over the first 20% of the chord. These data confirm that more forward-loaded airfoils are likely to be more sensitive, in terms of maximum lift degradation, to ice accretions in the leading-edge region.

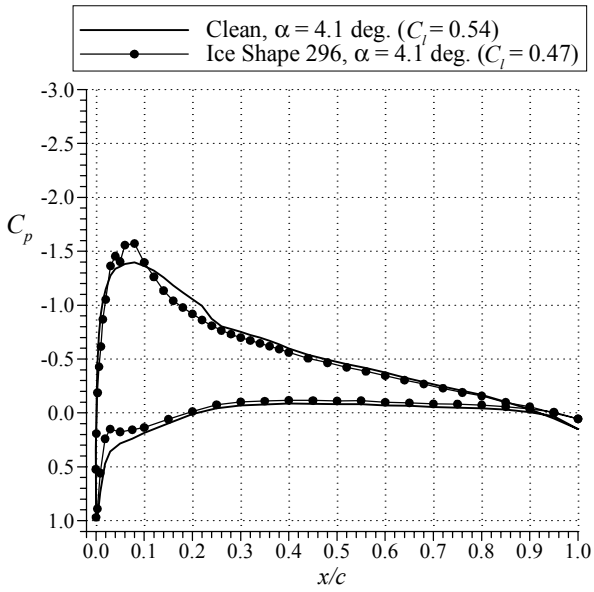

Fig. 19 Comparison of clean and iced pressure distributions for the NACA 23012 airfoil at matched angle of attack based on a clean $C_l \approx 0.5$.

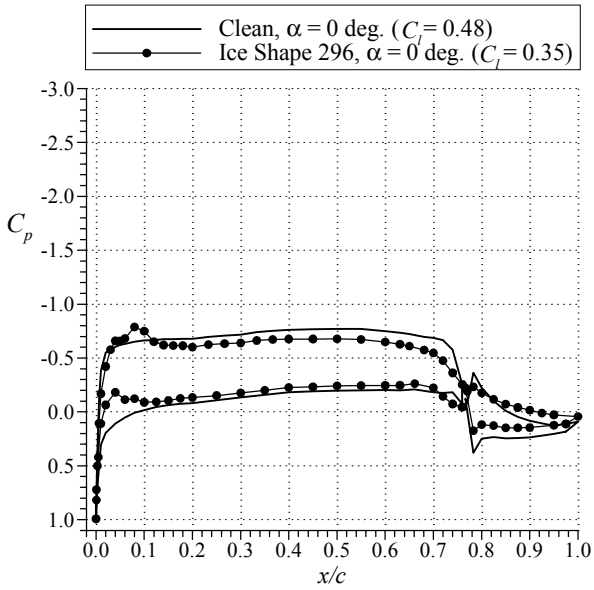

Fig. 20 Comparison of clean and iced pressure distributions for the NLF 0414 airfoil at matched angle of attack based upon a clean $C_l \approx 0.5$.

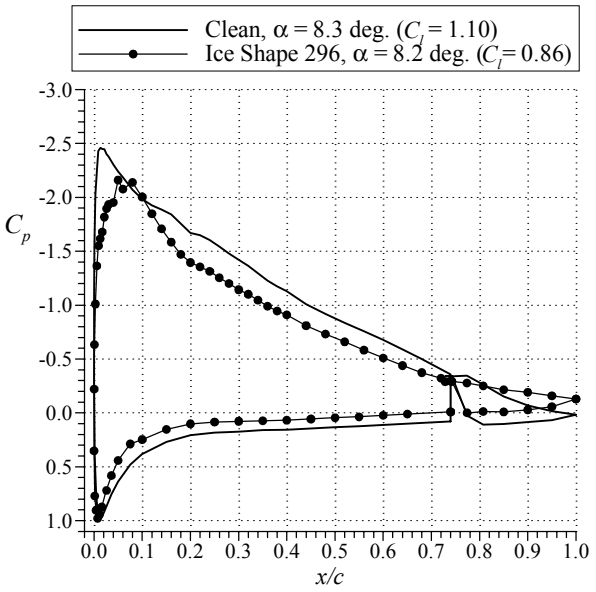

Fig. 21 Comparison of clean and iced pressure distributions for the NACA 3415 airfoil at matched angle of attack near stall in the iced configuration.

Comment on Reynolds Number Effects

The data from the Illinois wind tunnel presented here were all acquired at $Re = 1.8\times10^6$ and $Ma = 0.18$. Broeren *et al.*[5] investigated the effects of Reynolds number and Mach number over a range of $Re = 2.0\times10^6$ to 10.5×10^6 and $Ma = 0.10$ to 0.28. They found that there was only a small (less than 0.05 in C_l) increase in maximum lift coefficient between $Re = 2.0\times10^6$ and $Re = 3.5\times10^6$ for the NACA 23012 airfoil with each of the four intercycle ice accretions. The 40- and 80-grit sandpaper cases had about 0.10 increase in C_l. There was virtually no change in $C_{l,max}$ for Reynolds numbers larger than 3.5×10^6. Similar results were reported by Addy and Chung[14] for tests of glaze-ice simulations on an NLF 0414 airfoil. Also, a large glaze-ice simulation was tested on a multi-element super-critical airfoil by Morgan *et al.*[15] Performance measurements were carried out on the model in the cruise configuration over a Reynolds number range of 3.0×10^6 to 12.0×10^6 and only very minor changes in maximum lift were observed for the iced-airfoil case. Therefore, the results of the present study, should be applicable for higher Reynolds numbers. The caveat is that the clean maximum lift performance of the airfoils considered in this study is Reynolds number dependent. For example, Broeren *et al.*[5] reported a clean $C_{l,max}$ value for the NACA 23012 at $Re = 10.5\times10^6$ and $Ma = 0.21$ of 1.80. This is significantly higher than the value of 1.47 reported here for $Re = 1.8\times10^6$ and $Ma = 0.18$. Given that an intercycle iced-airfoil maximum lift coefficient

of 0.70 would be relatively invariant over this Reynolds number range, the performance penalty would be 61%, instead of the 52% value mentioned above. However, clean maximum lift values for these and other airfoils are more readily obtainable from historical data and/or computational methods.

Summary and Conclusions

The purpose of this paper was to evaluate the aerodynamic performance effects of intercycle ice accretions on the NACA 23012, NACA 3415 and NLF 0414 airfoils. These sections have geometries and pressure distributions that are substantially different. The intercycle ice shapes used in this study were adapted from an actual icing test on a 36-inch chord NACA 23012 airfoil model. The ice was simulated using various sizes of grit roughness and geometrically scaled to the 18-inch chord models used for these tests. Performance data were acquired for each of the airfoils with these ice simulations over a large angle of attack range at a Reynolds number of 1.8×10^6 and a Mach number of 0.18. Uniform roughness in the form of 80- and 150-grit sandpaper was also applied to the airfoil leading edge and tested.

The results for the ice simulations tested on the NACA 23012 airfoil were validated against previous testing of a 36-inch chord model that used castings of the actual ice shapes. Agreement between these tests was excellent and showed that the ice could be successfully scaled down by the ratio of the chord lengths and simulated with relatively simple methods. As shown in previous studies, the performance degradation resulting from the intercycle ice simulations was severe. For the NACA 23012 airfoil, the maximum lift coefficients were reduced to a range of 0.65 to 0.80 from a clean value of 1.47. Performance effects, in terms of maximum lift coefficient, were less severe for the other two airfoils. The NLF 0414 airfoil maximum lift coefficient was reduced to a range of 0.90 to 1.05 from a clean value of 1.34 with the intercycle ice simulations. These same simulations reduced the maximum lift coefficient of the NACA 3415 airfoil to a range of 0.85 to 0.95 from a clean value of 1.37.

The severe reductions in maximum lift for the NACA 23012 airfoil was related to the clean pressure distribution. This airfoil generated most of its lift from large suction pressures near the leading edge. The presence of the ice shape prevented the formation of these large suction pressures and hence the lift was substantially reduced. In the case of the other two airfoils, the pressure loading was distributed more uniformly along the chord and resulting maximum lift penalties were smaller. The lift penalties at low to moderate lift coefficients for the NLF 0414 and the NACA 3415 airfoils were more severe than for the NACA 23012. The former two airfoils' moderate pressure loading was more adversely affected at lower lift coefficients by the presence of the ice than for the front-loaded, NACA 23012 airfoil.

Tests conducted with the uniform roughness on the NACA 23012 airfoil were also validated against previous testing on a larger-chord model. These results also showed that these roughness heights could simply be scaled by the ratio of the chord lengths. The performance degradation resulting from the standard roughness was substantially less than that caused by the intercycle ice simulations. These effects, in terms of maximum lift, were more severe for the NACA 23012 and NACA 3415 airfoils, while the NLF 0414 was least affected. The sandpaper roughness was more than ten times smaller than the nominal height of the intercycle ice shapes. It is unclear if uniform roughness with similar heights would be an adequate ice simulation. Future testing should be conducted to determine what level of simulation provides acceptable aerodynamic results.

Acknowledgements

This work was supported in part under FAA grant DTFA MB 96-6-023 with Jim Riley as technical monitor. The authors wish to acknowledge Sam Lee, Ramesh Arakoni and Chris LaMarre of the University of Illinois for assistance in acquiring, processing and analyzing the data.

References

1. Shin, J., and Bond, T.H., "Surface Roughness Due to Residual Ice in the Use of Low Power Deicing Systems," NASA TM-105971, AIAA Paper 93-0031, Jan. 1993.

2. Albright, A.E., Kohlman, D.L., Schweikhard, W.G., and Evanich, P., "Evaluation of a Pneumatic Boot Deicing System on a General Aviation Wing Model," NASA TM-82363, June 1981.

3. Bowden, D.T., "Effect of Pneumatic De-Icers and Ice Formations on Aerodynamic Characteristics of an Airfoil," NACA TN-3564, Feb. 1956.

4. Jackson, D.G., and Bragg, M.B., "Aerodynamic Performance of an NLF Airfoil with Simulated Ice," AIAA Paper 99-0373, Jan. 1999.

5. Broeren, A.P., Addy, H.E., Jr., and Bragg, M.B., "Effect of Intercycle Ice Accretions on Airfoil Performance," AIAA Paper 2002-0240, Jan. 2002.

6. Lee, S., "Effect of Supercooled Large Droplet Icing on Airfoil Aerodynamics," Ph.D. Dissertation, Dept. of Aeronautical and Astronautical Engineering, Univ. of Illinois, Urbana, IL, 2001.

7. Lee, S., Kim, H.S., and Bragg, M.B., "Investigation of Factors that Influence Iced-Airfoil Aerodynamics," AIAA Paper 2000-0099, Jan. 2000.

8. Lee, S., and Bragg, M.B., "Effect of Simulated-Spanwise Ice Shapes on Airfoils: Experimental Investigation," AIAA Paper 99-0092, Jan. 1999.

9. Lee, S., and Bragg, M.B., "Experimental Investigation of Simulated Large-Droplet Ice Shapes on Airfoil Aerodynamics," *Journal of Aircraft*, Vol. 36, No. 5, Sept.-Oct., 1999, pp. 844-850.

10. Rae. W.H., and Pope, A., *Low-Speed Wind Tunnel Testing*, Wiley, New York, 1984, pp. 349-362, 449.

11. Kline, S.J., and McClintock, F.A., "Describing Uncertainties in Single-Sample Experiments," Mechanical Engineering, Vol. 75, Jan. 1953, pp. 3-8.

12. Coleman, H.W., and Steele, W.G., *Experimentation and Uncertainty Analysis for Engineers*, John Wiley and Sons, New York, 1989, pp. 40-118.

13. Broeren, A.P., and Bragg, M.B., "Effect of Residual and Intercycle Ice Accretions on Airfoil Performance," Report. No. DOT/FAA/AR-02/68, May 2002.

14. Addy, H.E., Jr., and Chung, J.J., "A Wind Tunnel Study of Icing Effects on a Natural Laminar Flow Airfoil," AIAA Paper 2000-0095, Jan. 2000.

15. Morgan, H.L., Ferris, J.C., and McGhee, R.J., "A Study of High-Lift Airfoils in the Langley Low-Turbulence Pressure Tunnel," NASA TM 89125, July 1987.